Original Paper

Integration of a fused silica capillary and in-situ Raman spectroscopy for investigating CO_2 solubility in n-dodecane at near-critical and supercritical conditions of CO_2

Jun-Liang Wang [a], Zi-Hao Song [a], Lin-Jun Li [a], Li-Li Yang [a], Quan-Yuan Wang [b], I-Ming Chou [c], Zhi-Yan Pan [a, *]

[a] College of Environment, Zhejiang University of Technology, Hangzhou, Zhejiang, 310032, China
[b] Hangzhou Academy of Environmental Protection, Hangzhou, Zhejiang, 310032, China
[c] Laboratory for Experimental Study Under Deep-sea Extreme Conditions, Institute of Deep-sea Science and Engineering, Chinese Academy of Sciences, Sanya, Hainan, 572000, China

ARTICLE INFO

ABSTRACT

To determine the solubility of CO_2 in n-dodecane at $T = 303.15-353.15$ K, $P \leq 11.00$ MPa, an integrated fused silica capillary and in-situ Raman spectroscopy system was built. The Raman peak intensity ratio (I_{CO_2}/I_{C-H}) between the upper band of CO_2 Fermi diad (I_{CO_2}) and the C−H stretching band of n-dodecane (I_{C-H}) was employed to determine the solubility of CO_2 in n-dodecane based on the calibrated correlation equation between the known CO_2 molality in n-dodecane and the I_{CO_2}/I_{C-H} ratio with $R^2 = 0.9998$. The results indicated that the solubility of CO_2 decreased with increasing temperature and increased with increasing pressure. The maximum CO_2 molality (30.7314 mol/kg) was obtained at 303.15 K and 7.00 MPa. Finally, a solubility prediction model ($\ln S = (P - A)/B$) based on the relationship with temperature (T in K) and pressure (P in MPa) was developed, where S is CO_2 molality, $A = -8 \times 10^{-6}T^2 + 0.0354T - 8.1605$, and $B = 0.0405T - 10.756$. The results indicated that the solubilities of CO_2 derived from this model were in good agreement with the experimental data.

1. Introduction

Recently, mitigating climate change by reducing greenhouse gas emissions has become a global focus, and the ability to reduce CO_2 emissions accordingly has become an urgent task. Carbon capture and storage (CCS) has been widely recognized as a viable method to mitigate carbon emissions (Cormos, 2012; Peng et al., 2013; You et al., 2014; Li et al., 2016; Sun et al., 2017). Among all the storage methods, CO_2 geological storage has a direct effect on emission reduction and is considered to be the most potential storage method (Leung et al., 2014). Geological storage sites include oil and gas fields, saline aquifers, and deep coal seams (Michael et al., 2010). Injection of CO_2 in oil and gas fields can not only achieve CO_2 emission reductions but also enhance oil recovery (EOR) (Liu et al., 2016). Currently, many countries have conducted field tests of CO_2 flooding in oil fields using mature CO_2-EOR technology (Awan et al., 2008; Hill et al., 2013; Lacy et al., 2013; Lv et al., 2015).

The dissolution of CO_2 in oil can result in oil swelling and viscosity reduction, thereby enhancing oil recovery. CO_2 solubility data are one of the major parameters to determine the performance of CO_2-EOR process (Mosavat et al., 2014). The solubility of CO_2 in crude or simulated oil (of which the primary components are alkanes) systems at different temperatures and pressures have been investigated previously. Chung et al. (1988) and Henni et al. (1996) employed gas chromatography to analyze the solubility of CO_2 in heavy oil at temperatures of 297, 333 and 391 K and pressures of up to 34.5 MPa, and in n-dodecane at 313, 353, and 393 K and 0−9.6 MPa. Kavousi et al. (2014) studied CO_2 solubility in heavy oils with different viscosities using the pressure drop method at pressures of 1.73−4.48 MPa and temperatures of 295−305 K.

Previous methods for investigating the solubility of CO_2 in crude/simulated oil systems at high pressure conditions have been performed primarily with the PVT apparatus (Lay et al., 2006; Nourozieh et al., 2013), equilibrium liquid sampling analysis (Yang

* Corresponding author.
  E-mail address: panzhiyan@zjut.edu.cn (Z.-Y. Pan).

et al., 2013), and chromatography (Forte et al., 2011). Although these methods offer distinct advantages, there continue to be some shortcomings. For example, the temperature and pressure ranges of the entire system of the PVT apparatus are limited, and the equilibrium liquid sampling analysis easily changes the original temperature and pressure conditions during the sampling process and upsets the system balance. Analysis of CO_2 quantity at the equilibrium point is the key to determine the solubility of CO_2 in crude oil and simulated crude oil. The equilibrium points of these methods generally are judged according to the pressure or the bubble point. It takes plenty of time to reach phase equilibrium because of the higher viscosity of the crude or simulated oil, which leads to an inaccurate judgment of the equilibrium condition in subjective or experimental environments (Mosavat et al., 2014; Han et al., 2015; Gui et al., 2017). In addition, the temperatures and pressures investigated in previous studies frequently have been confined to narrow ranges. Raman spectroscopy is an effective optical analysis method that is noninvasive, sensitive, and fast. (Liu et al., 2012; Belgodere et al., 2015). Therefore, Raman spectroscopy has been used in numerous studies of solubility measurements (e.g., Caumon et al., 2017; Wang et al., 2018).

The change in Raman peak intensity (peak height or peak area) ratio between two species in a fluid reflects variations in their relative quantities. For example, Wang et al. (2019) and Guo et al. (2014) demonstrated that the ratio between the upper band of CO_2 Fermi diad and the O–H stretching band of water in homogenous solutions could be used to determine the solubility of CO_2 in water at various pressure-temperature conditions. Similarly, the ratio between the upper band of CO_2 Fermi diad and the C–H stretching band of n-dodecane enables quantification of CO_2 solubility in n-dodecane.

In this study, to determine the solubility of CO_2 in n-dodecane at temperatures of 303.15–335.50 K and pressures up to 11.0 MPa, an integrated fused silica capillary and in-situ Raman spectroscopy system was built (Pan et al., 2013a, 2013b; Wang et al., 2017a, 2017b). n-dodecane, one of the primary components of crude oil, was used as a simulated oil in this experiment. The physical properties of n-dodecane ($\rho = 753$ kg/m^3, $\mu = 1.36$ cp at 298.15 K, and atmospheric pressure) are similar to those of light crude oil (Bei et al., 2018). The Raman spectra of the system with CO_2 dissolved in n-dodecane are presented in Fig. 1. It shows that the main Raman peaks (2800–3000 cm^{-1}) of n-dodecane do not coincide with the CO_2 Fermi diad upper band (1385 cm^{-1}) and its minor peaks at 1250–1500 cm^{-1} do not block the upper Fermi diad band of CO_2 at 1385 cm^{-1}. Therefore, any influence of the peaks of the n-dodecane at 1250–1500 cm^{-1} to the intensity of the upper Fermi diad band of CO_2 at 1385 cm^{-1} can be ignored. In this study, the ratio between the upper band of CO_2 Fermi diad and the C–H stretching band of n-dodecane (I_{CO_2}/I_{C-H}) was used to determine the CO_2 solubility in n-dodecane, based on the calibrated correlation equation between the known CO_2 molality in n-dodecane and the I_{CO_2}/I_{C-H} ratio. Finally, a CO_2 solubility model based on its relationship with temperature and pressure was developed.

2. Materials and methods

2.1. Materials

Table 1 presents the chemicals used in this work. CO_2 with a purity of 99.995% was purchased from the Shanghai Pujiang Special Gas Co., Ltd. (Shanghai, China). n-dodecane with a purity of 99.00% was supplied by Aladdin Chemical Reagent Co., Ltd. (Shanghai, China). All of the chemicals were purchased commercially and were used as received with no further purification. The silica capillary tubing with polyimide coating was purchased from Polymicro
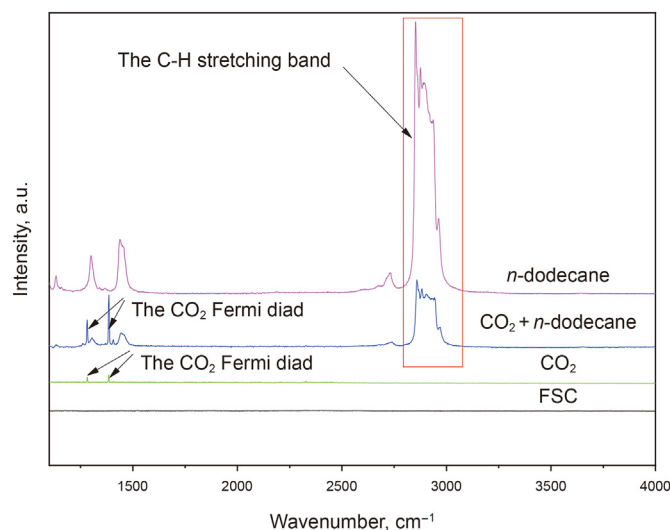

Fig. 1. Raman spectra of CO_2, n-dodecane, and fused silica capillary (FSC).

Technologies, LLC (Phoenix, AZ, USA) with an outer diameter of 665 μm and inner diameter of 300 μm. All of the valves and high-pressure stainless-steel tubes were purchased from the Nantong Huaxing Petroleum Instrument Co., Ltd. (Nantong, Jiangsu, China).

2.2. Apparatus

An experimental setup was built to measure the solubility of CO_2 in n-dodecane at 303.15–353.15 K and up to 11.00 MPa (Fig. 2). The apparatus primarily consisted of a fused silica capillary (FSC) and the balance kettle observation window, combined with a heating-cooling stage (CAP500, Linkam Scientific Instruments, Tadworth, UK), a confocal Raman spectrometer (Horiba JobinYvon, HR800, HORIBA FRANCE, Palaiseau, France), a horizontal phase equilibrium kettle with a magnetic stirrer, a manual pressure pump (JY-80, Jiangsu, China), a 70.00 MPa pressure sensor, a magnetic circulating pump, and a quantitative pump (30.00 MPa full scale). A circulation line was formed by the FSC connected to a circulating pump and a phase equilibrium kettle with an electric heating jacket, which could adjust the temperature of the fluid in the kettle. Controlled the temperature within the FSC utilizing a heating-cooling stage in conjunction with a digital temperature controller (accurate to 0.1 K). The pressure of the phase equilibrium kettle was adjusted using a manual pressure pump connected to a pressure transducer (70.00 MPa full scale, accurate to ±0.25% FS) and an electric heater connected to a digital temperature controller (accurate to 0.1 K). Measurements of pressures in the quantitative pump were achieved by using a pressure transducer (30.00 MPa full scale, accurate to ±0.25% FS).

2.3. Experimental procedures

The procedure for measuring the solubility of CO_2 in n-dodecane at different temperatures and pressures followed two steps: (1) determination of the relationship between the known CO_2 molality and the Raman peak intensity ratio of the upper band of CO_2 and n-dodecane in a homogeneous CO_2/n-dodecane system; and (2) measurement of the Raman peak intensity of the upper band of CO_2 and n-dodecane in a CO_2-saturated CO_2/n-dodecane system.

The procedures for the first step included the following: (1) Valve 11 was opened, and a certain amount of n-dodecane was fed into the phase equilibrium kettle using the liquid sampler at room

Table 1
CAS registry number, source, mass fraction purity and molecular weight of the chemicals used in this work.

Component	CAS Reg. No.	Suppliers	Purity, wt%	M, g·mol^{-1}
CO_2	124-38-9	Pujiang special gas Co., Ltd.	≥ 99.995[a]	44.01
n-dodecane	112-40-3	Aladdin Chemical Reagent Co., Ltd.	≥ 99.0[a]	170.33

[a] Purities given by supplier; no further purification was performed.
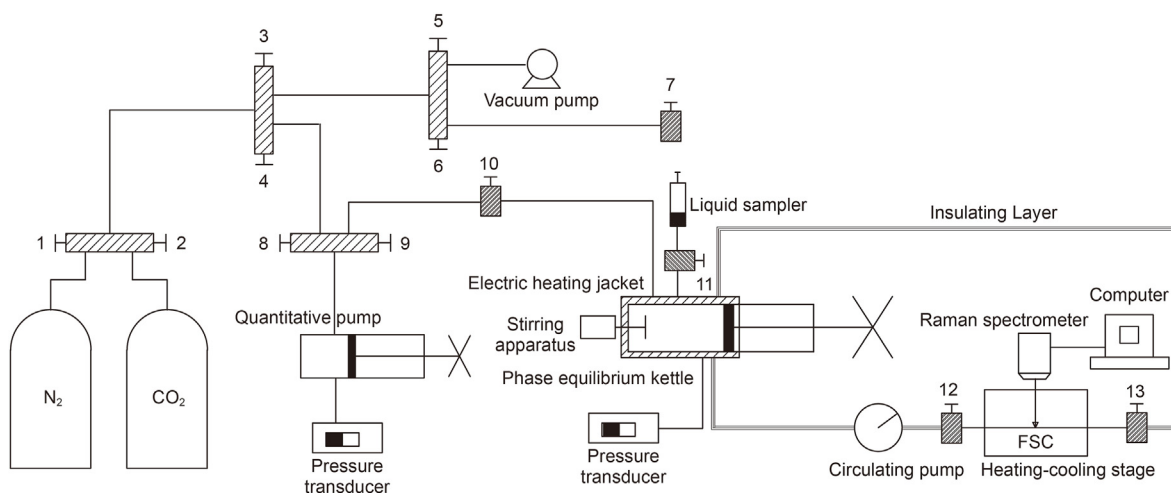
Fig. 2. Schematic diagram of the CO_2 + n-dodecane solubility measurement system. 1 to 13 are high-pressure valves. FSC = fused silica capillary.

temperature (about 293.15 K). Then, the valve was closed; (2) Valves 2, 4, and 8 were opened, and the quantitative CO_2, which was estimated in advance, was charged into the quantitative pump, and then the three valves were closed. The CO_2 was pressed into the cell using the quantitative pump, and valves 9 and 10 were successively opened and closed. During this step, a pressure transducer was used to measure the initial and final pressures, and a digital temperature controller was used to measure the initial and final temperatures. The void volume of the quantitative pump and the pipe gap between the quantitative pump and the phase equilibrium kettle was known. Thus, using the Peng-Robinson equation to calculate the amount of CO_2 which was injected into the system (accurate to ±0.13%); (3) The

mixture was slowly compressed to 30.00 MPa using a manual pressure pump that was connected to the phase equilibrium kettle. The stirring device was used for several hours to accelerate the CO_2 dissolution; (4) The circulating pump was turned on for approximately 30 min to ensure the homogeneity of the solution in the circulation line, and then it was turned off. The Raman spectrum of a homogeneous CO_2/n-dodecane solution was collected; (5) Repeated step (4) until the deviation of the Raman peak intensity ratio between the upper band of CO_2 Fermi diad and the C–H stretching band of the n-dodecane from previous measurement could be neglected, proving that the system had reached dissolution equilibrium; (6) The temperature or pressure was changed using the same procedures to ensure that the system reached dissolution
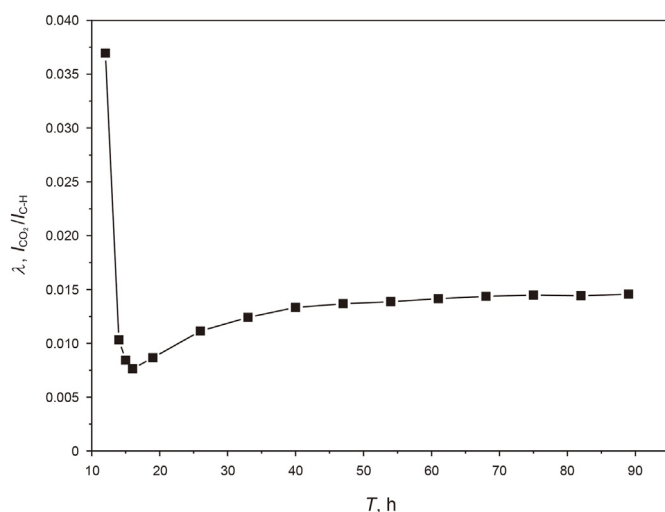
Fig. 3. Variation in the Raman peak intensity ratio of the CO_2 + n-dodecane system with time (T = 293.15 K, P = 6.67 MPa, x_{CO_2} = 0.1071 mol/kg).
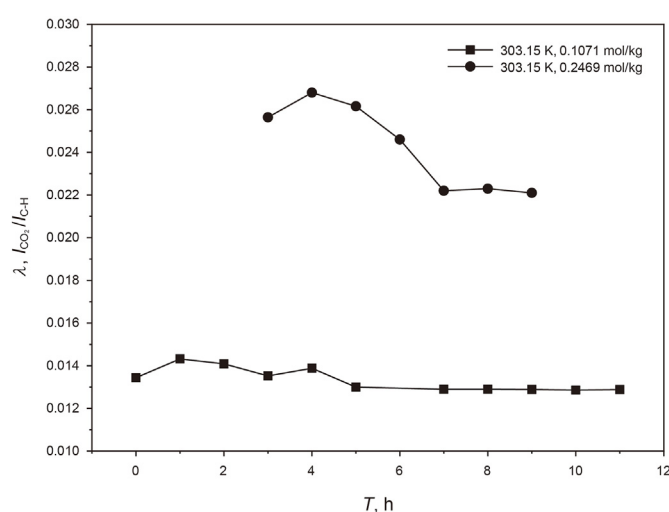
Fig. 4. The change in the CO_2 + n-dodecane Raman peak intensity ratio with time under different CO_2 concentrations at 303.15 K.
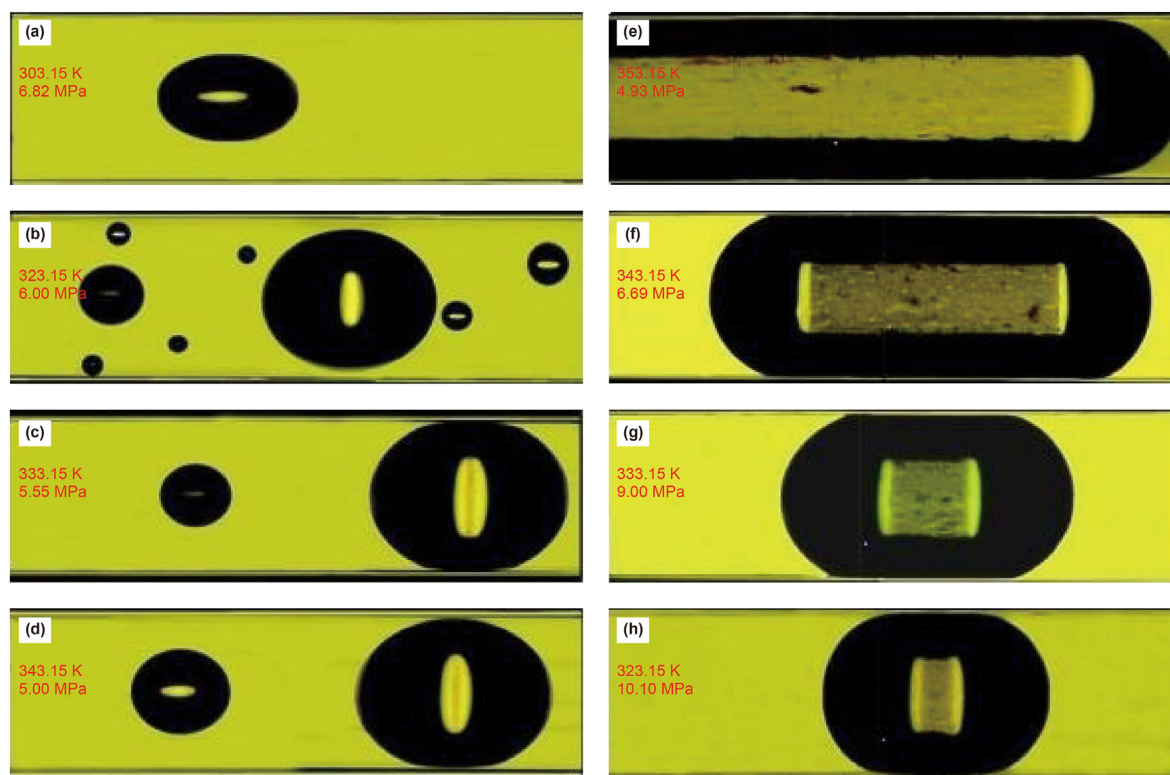
Fig. 5. Changes in the CO_2-saturated solution during heating and depressurization (a) → (d), and cooling and pressurization (e) → (h) in a FSC.
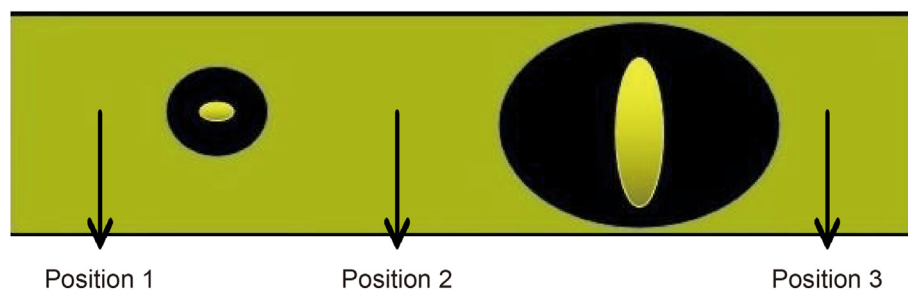

Fig. 6. Three positions for Raman spectroscopic measurements in the CO_2-saturated solution in a FSC.

equilibrium, and the Raman spectra of the solution were collected at different pressures and temperatures. (7) The CO_2 molality was changed, and repeated steps (2)–(6); (8) The experiment was repeated to obtain the Raman spectra of the CO_2-containing homogeneous solution under different pressures and at temperatures of 303.15–353.15 K. The CO_2 molality was plotted versus the Raman peak intensity ratio of the CO_2/n-dodecane solution, and the equation of the calibrated line was obtained.

The procedures for measuring the Raman peak intensity ratio of CO_2 and n-dodecane and judging the phase equilibrium in the saturated CO_2/n-dodecane system are the same as those for the homogeneous CO_2/n-dodecane system. After reaching phase equilibrium, some bubbles appeared as the temperature of the system was increased or as the pressure was decreased in the saturated CO_2/n-dodecane system. The Raman peak intensities of the upper band of CO_2 Fermi diad and the C−H stretching band of the n-dodecane under different temperature-pressure conditions (303.15–353.15 K, 0–15.00 MPa) were determined for the solution

near the CO_2 bubbles (approximately 100 μm from the edge of the CO_2 bubbles), and the Raman peak intensity ratios were calculated.

In the experiment, a JY/Horiba LabRam HR800 system equipped with a frequency-doubled Nd:YAG 531.95 nm laser with 20 mW of output laser power to collect the Raman spectra was employed. In addition, a charge coupled device (CCD) detector (multichannel, air cooled) was utilized to analyze the CO_2 + n-dodecane system in situ. Under various temperature-pressure conditions, the Raman spectra of the system in the range of 1100−4000 cm^{-1} were collected to obtain the peak intensity ratio of the CO_2 Fermi diad upper band to the C−H stretching band of the n-dodecane. The acquisition time was 20 s with two accumulations. The Raman peak intensity ratio of each group of temperature-pressure-composition (T-P-x) conditions was measured five times and the average value was invoked as the experimental datum.

The details of how to determine the molality of CO_2 (x) have been reported in our previous study (Wang et al., 2019). Raman peak intensity (height) ratio (λ) was calculated using Eq. (1).

Table 2
Raman peak intensity ratios of the CO_2 + n-dodecane system at three positions in the FSC under three different temperature-pressure conditions.

T, K	P, MPa	Raman peak intensity ratio			SD^a
		Position 1	Position 2	Position 3	
313.15	3.61	0.1737	0.1732	0.1726	0.0006
323.15	4.85	0.2317	0.2329	0.2325	0.0006
343.15	9.00	0.5394	0.5478	0.5394	0.0048
353.15	10.56	0.6709	0.6648	0.6744	0.0049

[a] The standard deviation (SD) for the mean values of the Raman peak intensity ratio (λ) was calculated from the three Raman spectra collected.

$$\lambda = \frac{I_{CO_2}}{I_{C-H}} \tag{1}$$

where I_{CO_2} is the Raman peak intensity (height) of the CO_2 Fermi diad upper band, I_{C-H} is the Raman peak intensity (height) of the C−H stretching band of the n-dodecane, and the baseline is subtracted during the calculation.

Table 3
The Raman peak intensity ratio of the CO_2 + n-dodecane system for the same CO_2 molality and different temperature-pressure conditions.[a]

x_{CO_2}, mol/kg	T, K	P, MPa	Peak intensity ratio	SD
0.1071	303.15	4.99	0.0127	0.0001
		7.60	0.0129	
		10.08	0.0128	
		15.03	0.0130	
	313.15	4.56	0.0126	0.0003
		9.21	0.0129	
		10.08	0.0128	
		14.78	0.0132	
	323.15	3.61	0.0129	0.0004
		8.64	0.0128	
		11.25	0.0125	
		14.95	0.0135	
0.3859	313.15	2.89	0.0334	0.0003
		6.56	0.0340	
		10.12	0.0337	
		12.70	0.0338	
	323.15	2.34	0.0337	0.0003
		4.85	0.0330	
		9.38	0.0335	
		12.69	0.0336	
	333.15	2.19	0.0326	0.0005
		5.38	0.0333	
		8.77	0.0337	
		12.70	0.0333	
0.6450	333.15	3.67	0.0547	0.0010
		6.25	0.0556	
		9.57	0.0532	
		13.98	0.0551	
	343.15	3.67	0.0527	0.0014
		6.25	0.0541	
		9.57	0.0560	
		13.98	0.0551	
	353.15	2.34	0.0528	0.0010
		4.85	0.0537	
		9.38	0.0543	
		12.69	0.0551	

[a] Standard uncertainties u are $u(T) = 0.01$ K, $u(P) = 0.039$ MPa, and the uncertainties of CO_2 molality are estimated based on the SD of calculation.

3. Results and discussion

3.1. Determination of the phase equilibrium of the CO_2 + n-dodecane system

The prerequisite for determining the solubility of CO_2 in n-dodecane is the phase equilibrium of the CO_2 + n-dodecane system. Confocal Raman spectroscopy can be utilized to quantitatively monitor the concentration of gases in aqueous solutions because the band intensity of an active Raman species is proportional to its concentration in a fluid (Han et al., 2015; Wang et al., 2017a). Therefore, in this study, the peak intensity ratio of CO_2 Fermi diad upper band to the C−H stretching band of n-dodecane was employed to verify whether the system reached thermodynamic equilibrium under a particular *T-P-x* condition.

3.1.1. Phase equilibrium determination of the CO_2 + n-dodecane system during homogenization

After feeding quantitative CO_2 into cells at room temperature, Raman spectroscopy was used to track the Raman peak intensity of the CO_2 and the n-dodecane in the FSC in real time and calculated the peak intensity ratio to understand the mass transfer of CO_2 in the system. Variation in the Raman peak intensity ratio of the CO_2 + n-dodecane with time at 293 K and 6.67 MPa is shown in Fig. 3. It can be seen that the Raman peak intensity ratio was relatively high during the preliminary stage, but it decreased rapidly after the stirring device was turned on. During continuous stirring of the fluid, the CO_2 gradually dissolved in the n-dodecane, and the Raman peak intensity ratio increased and finally stabilized around 68 h, indicating the system had nearly reached phase equilibrium.

After the system reached the phase equilibrium for this sample fluid with known x_{CO_2}, the temperature of the system was adjusted and the Raman peak intensity of the system was measured at a new *T-P* condition. While the deviation of the obtained Raman peak intensity ratio from the previous measurement was negligible, it can be considered that the system has reached phase equilibrium at this time. Fig. 4 shows that the time required to reach the phase equilibrium was approximately 7 h at 303.15 K for CO_2 concentrations of 0.1071−0.2469 mol/kg.

3.1.2. Phase equilibrium determination of a CO_2-saturated solution

While increasing the system temperature or decreasing the system pressure from the CO_2-saturated equilibrium *T-P* condition, bubbles could be formed in the CO_2 + n-dodecane system due to the amount of available CO_2 is more than the solubility value. Fig. 5 shows the formation and growth of CO_2 bubble(s) during heating and decompression (a→d), and the shrinkage of a CO_2 bubble during cooling and pressurization (e→h). By adjusting the system to a specific temperature and pressure, the size of the bubbles in the CO_2 + n-dodecane system can be observed under a microscope. When the sizes of bubbles did not change within 1 h, in order to further ensure the phase equilibrium of the system, Raman spectra at positions 1, 2, and 3 were collected (Fig. 6) and the Raman peak intensity ratios of the upper band of CO_2 Fermi diad and the C−H stretching band of n-dodecane were calculated. Results, listed in Table 2 for three *T-P* conditions, show that the system had reached phase equilibrium.

To confirm the feasibility of the method, the peak intensities at position 2 were continuously tracked every 20 min for 2 h after phase equilibrium was reached to determine whether the phase balance was reached in this state. As shown in Fig. 7, the Raman spectra of the CO_2 + n-dodecane system were acquired at position 2 at 333.15 K and 5.55 MPa from 0 to 120 min, and the peak intensity ratios were found to be 0.2247, 0.2278, 0.2309, 0.2313, and
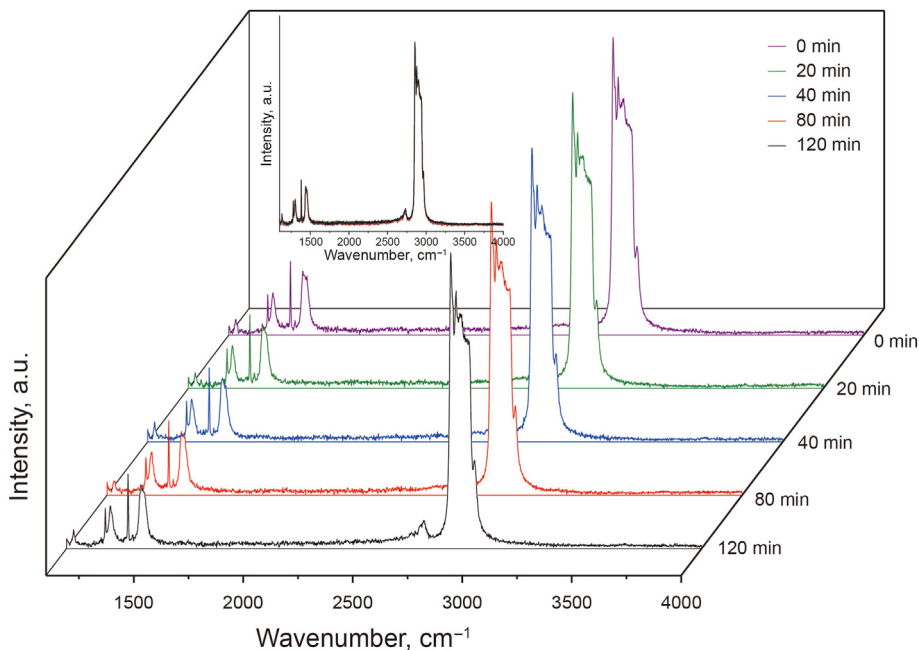
Fig. 7. Raman spectra of the CO_2 + n-dodecane system at 333.15 K and 5.55 MPa from 0 to 120 min after phase equilibrium was reached.

0.2315. The variations in the peak intensity ratio became increasingly smaller as time went on, which were negligible during these times.

3.2. The relationship between the CO_2 concentration and the Raman peak intensity ratio in the CO_2 + n-dodecane system

After reaching phase equilibrium in a homogeneous CO_2 system, Raman spectroscopy was used to measure the peak intensity ratio of the system at different pressures and temperatures. As shown in Table 3, for the same CO_2 molality and temperatures, the changes in the Raman peak intensity ratio of the system with increasing pressure were very slight, with standard deviations of less than 0.0015, which were negligible. Thus, pressure had little effect on

the peak intensity ratio. According to Table 4, the Raman peak intensity ratio of the system slightly decreased with increasing temperature at a constant CO_2 concentration and constant pressure, but the standard deviation of the peak intensity ratio from 303.15 to 353.15 K was less than 0.0007 for each x_{CO_2}, which indicated that the temperature also had little effect on the peak intensity ratio. As a result, the peak intensity ratio of the homogeneous solution did not depend on temperature and pressure within the range of these experimental conditions. Therefore, the linear relationship between the CO_2 molality and the CO_2 + n-dodecane Raman intensity ratio does not need to consider the effect of temperature and pressure.

In this experiment, the average value of the Raman peak intensity ratio of the CO_2 + n-dodecane system at the same CO_2 molality and under design temperature conditions was used to establish a correlation equation for CO_2 molality. As shown in Fig. 8 (the data see Table S1), there was a positive correlation ($R^2 = 0.9998$) between the CO_2 molality and the Raman peak intensity ratio of the CO_2 + n-dodecane system. The correlation equation is as following:

$$\lambda = 0.0845x + 0.0023 \tag{2}$$

where λ is the peak intensity ratio of the CO_2 + n-dodecane system; and x is the molality of CO_2 (mol/kg).
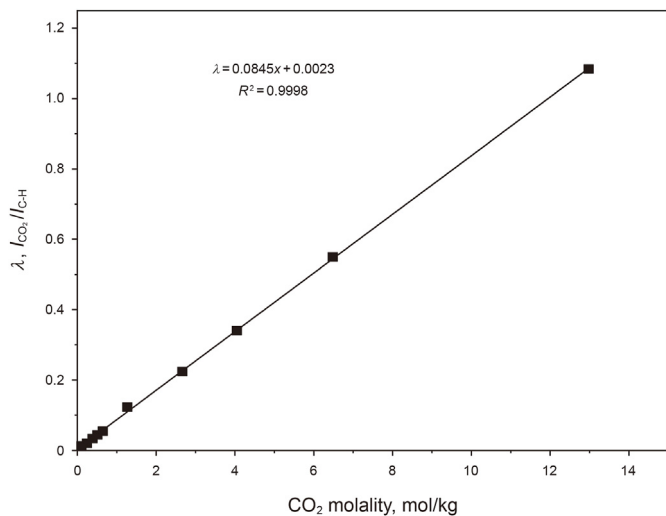

Fig. 8. The relationship between CO_2 molality and the Raman peak intensity ratio between the upper band of CO_2 Fermi diad and n-dodecane derived from spectra collected from homogeneous CO_2/n-dodecane solutions.

Table 4
Raman peak intensity ratio of a homogeneous solution at different temperatures and CO_2 molality.

x_{CO_2}, mol/kg	T, K						SD
	303.15	313.15	323.15	333.15	343.15	353.15	
0.1071	0.0129	0.0128	0.0128	0.0127	0.0128	0.0128	0.0001
0.2469	0.0223	0.0221	0.0200	0.0218	0.0221	0.0218	0.0002
0.3859	0.0341	0.0338	0.0340	0.0338	0.0335	0.0333	0.0003
0.5079	0.0453	0.0442	0.0447	0.0439	0.0436	0.0433	0.0007
0.6450	0.0556	0.0553	0.0552	0.0551	0.0547	0.0543	0.0005

Table 5
Raman peak intensity ratio and solubility of the CO_2 in n-dodecane at 303.15–353.15 K and 1.00–11.00 MPa[a].

T, K	P, MPa	Raman peak intensity ratio (λ[b]±SD)	Solubility±SD, mol/kg	T, K	P, MPa	Raman peak intensity ratios (λ[b]±SD)	Solubility±SD, mol/kg
303.15	1.08	0.0558 ± 0.0005	0.6331 ± 0.0446	313.15	1.08	0.0518 ± 0.0004	0.5858 ± 0.0434
	2.14	0.1064 ± 0.0009	1.2320 ± 0.0493		2.59	0.1054 ± 0.0006	1.2201 ± 0.0458
	3.00	0.1787 ± 0.0007	2.0876 ± 0.0470		3.61	0.1731 ± 0.0009	2.0213 ± 0.0493
	3.47	0.2426 ± 0.0015	2.8438 ± 0.0564		4.10	0.2296 ± 0.0013	2.6899 ± 0.0541
	4.65	0.5213 ± 0.0029	6.1420 ± 0.0730		5.00	0.3659 ± 0.0019	4.3030 ± 0.0612
	5.03	0.6764 ± 0.0032	7.9775 ± 0.0765		6.13	0.6522 ± 0.0024	7.6911 ± 0.0671
	5.75	1.1051 ± 0.0038	13.0509 ± 0.0836		6.36	0.7307 ± 0.0039	8.6201 ± 0.0848
	6.00	1.2945 ± 0.0053	15.2923 ± 0.1014		7.55	1.4502 ± 0.0062	17.1349 ± 0.1120
	6.19	1.5102 ± 0.0064	17.8450 ± 0.1144		7.79	1.6121 ± 0.0087	19.0509 ± 0.1416
	6.40	1.6823 ± 0.0078	19.8817 ± 0.1310		8.00	1.8432 ± 0.0095	21.7858 ± 0.1511
	6.65	2.0811 ± 0.0115	24.6012 ± 0.1748		8.35	2.2505 ± 0.0124	26.6059 ± 0.1854
	6.82	2.3505 ± 0.0132	27.7893 ± 0.1949		8.45	2.3619 ± 0.0138	27.9243 ± 0.2020
	7.00	2.5991 ± 0.0125	30.7314 ± 0.1866		–	–	–
323.15	1.08	0.0485 ± 0.0003	0.5467 ± 0.0422	333.15	0.99	0.0460 ± 0.0002	0.5172 ± 0.0410
	3.00	0.1080 ± 0.0007	1.2509 ± 0.0470		3.27	0.1054 ± 0.0005	1.2201 ± 0.0446
	3.97	0.1626 ± 0.0005	1.8970 ± 0.0446		4.49	0.1582 ± 0.0006	1.8450 ± 0.0458
	4.12	0.1783 ± 0.0008	2.0828 ± 0.0481		5.12	0.1913 ± 0.0013	2.2367 ± 0.0541
	4.85	0.2323 ± 0.0010	2.7219 ± 0.0505		5.55	0.2314 ± 0.0009	2.7112 ± 0.0493
	5.86	0.3515 ± 0.0015	4.1325 ± 0.0564		6.36	0.3011 ± 0.0015	3.5361 ± 0.0564
	7.85	0.8662 ± 0.0029	10.2237 ± 0.0730		6.89	0.3753 ± 0.0019	4.4142 ± 0.0612
	8.69	1.2787 ± 0.0032	15.1053 ± 0.0765		8.38	0.6513 ± 0.0025	7.6805 ± 0.0683
	9.13	1.5491 ± 0.0063	18.3053 ± 0.1132		9.00	0.7904 ± 0.0033	9.3266 ± 0.0777
	9.54	1.7695 ± 0.0084	20.9136 ± 0.1381		–	–	–
	9.88	2.1087 ± 0.0126	24.9278 ± 0.1878		–	–	–
	10.10	2.3489 ± 0.0137	27.7704 ± 0.2008		–	–	–
	10.25	2.4954 ± 0.0135	29.5041 ± 0.1984		–	–	–
343.15	1.01	0.0454 ± 0.0002	0.5101 ± 0.0410	353.15	1.00	0.0436 ± 0.0001	0.4888 ± 0.0399
	3.79	0.1095 ± 0.0006	1.2686 ± 0.0458		4.13	0.1044 ± 0.0006	1.2083 ± 0.0458
	5.00	0.1608 ± 0.0008	1.8757 ± 0.0481		4.93	0.1372 ± 0.0005	1.5964 ± 0.0446
	6.25	0.2325 ± 0.0012	2.7243 ± 0.0529		5.75	0.1658 ± 0.0012	1.9349 ± 0.0529
	6.89	0.2798 ± 0.0013	3.2840 ± 0.0541		6.69	0.2202 ± 0.0015	2.5787 ± 0.0564
	7.94	0.3824 ± 0.0017	4.4982 ± 0.0588		8.40	0.3463 ± 0.0022	4.0710 ± 0.0647
	9.00	0.5343 ± 0.0026	6.2959 ± 0.0694		9.47	0.4857 ± 0.0026	5.7207 ± 0.0694
	9.40	0.6154 ± 0.0034	7.2556 ± 0.0789		10.00	0.5660 ± 0.0024	6.6710 ± 0.0671
	10.00	0.7560 ± 0.0032	8.9195 ± 0.0765		10.17	0.6022 ± 0.0034	7.0994 ± 0.0789
	–	–	–		10.56	0.6712 ± 0.0038	7.9160 ± 0.0836
	–	–	–		10.62	0.6745 ± 0.0033	7.9550 ± 0.0777
	–	–	–		10.87	0.7092 ± 0.0036	8.3657 ± 0.0813

[a] Standard uncertainties u are u(T) = 0.01 K, u(P) = 0.039 MPa.
[b] The arithmetic means of the five measurements of the Raman peak intensity ratio of the CO_2 + n-dodecane system at the T - P conditions.
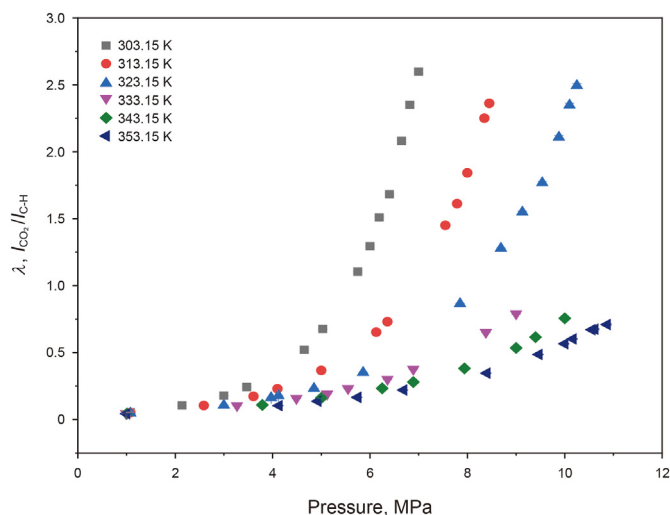

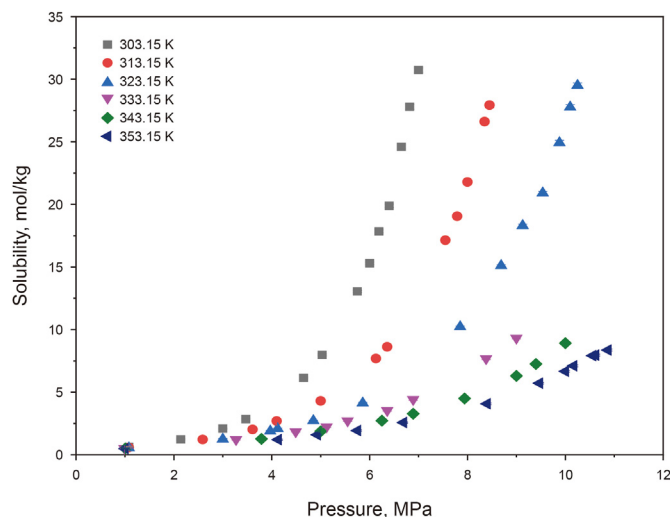**Fig. 9.** Raman peak intensity ratios of the CO_2 + *n*-dodecane system at 303.15–353.15 K and 1.00–11.00 MPa.

Fig. 10. Solubility of CO_2 in *n*-dodecane at 303.15–353.15 K and 1.00–11.00 MPa.
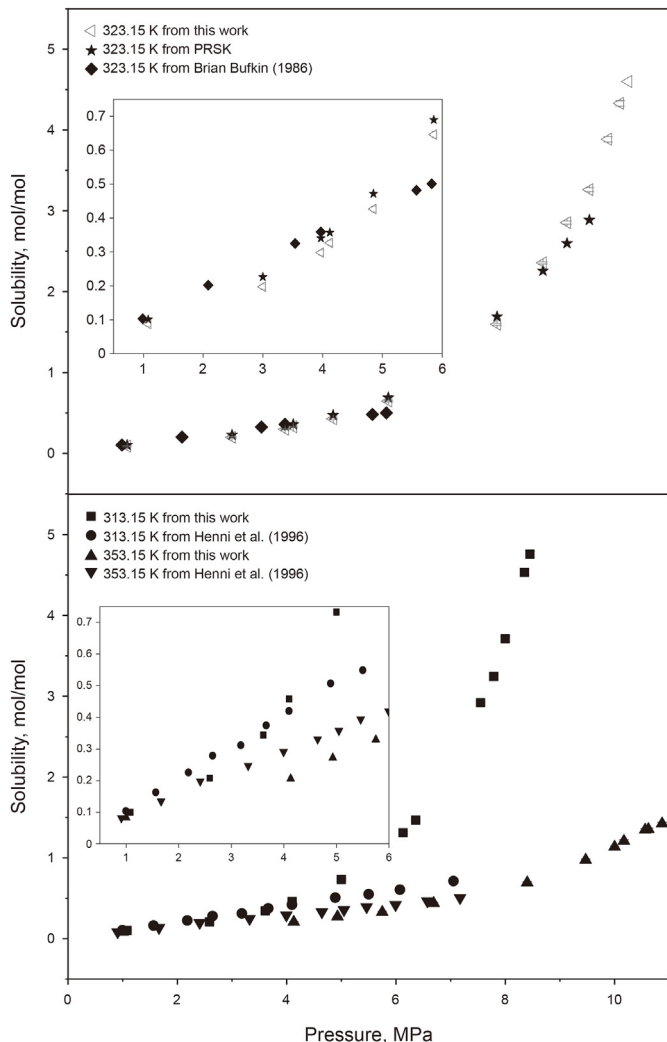
Fig. 11. Comparison of the CO_2 solubilities in n-dodecane obtained in this study with those reported previously.

Fig. 12. Comparison of the experimental values of CO_2 solubility in n-dodecane with those calculated from a model.

3.3. Determination of the solubility of CO_2 in n-dodecane

The solubility of the system based on the peak intensity ratio of the system under different temperature and pressure conditions in the saturated solution could be calculated from the relationship between the CO_2 molality and the peak intensity ratio of the CO_2 + n-dodecane (Eq. (2)). At temperatures of 303.15−353.15 K and pressures of 1.00−11.00 MPa, the Raman spectra of CO_2 and n-dodecane in CO_2-saturated solution were collected, and the peak intensity ratios were calculated (shown in Table 5 and plotted in Fig. 9). The reproducibility of peak intensity ratio is characterized by relative standard deviation, which ranges from 0.23% to 0.90%, it proved that samples were appropriate to be analyzed by this method with satisfactory results in our works.

As shown in Fig. 10, the solubility of the CO_2-saturated solution decreased with increasing temperature and increased with increasing pressure. The maximum solubility obtained in this study is 30.7314 mol/kg at 303.15 K and 7.00 MPa.

According to Fig. 10, the CO_2 solubility in n-dodecane gradually increased with increasing pressure and decreased with increasing temperature. At lower pressure, CO_2 had a weaker solubility in n-dodecane, and the solubility increased nearly linearly with increasing pressure. As the pressure increased, the distance
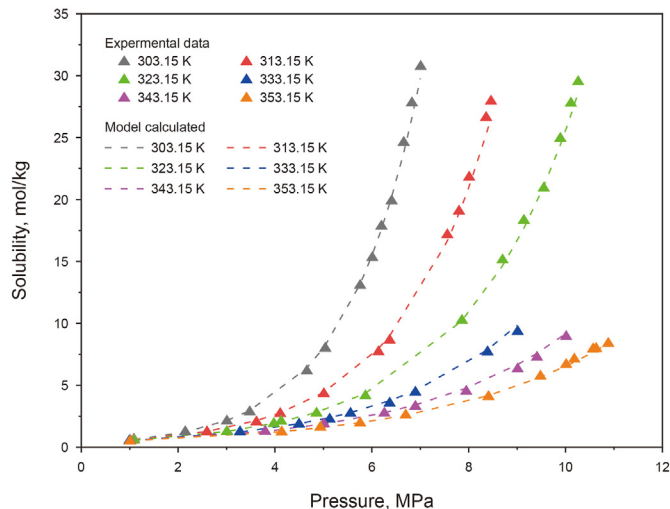
between the CO_2 and the n-dodecane molecule decreased, and the interaction force increased and gradually approached the force between the n-dodecane molecules, causing the CO_2 solubility to increase (Yang et al., 2013). In particular, the CO_2 solubility in n-dodecane-rich liquid phase changes significantly for pressures and temperatures close to the critical pressure and temperature of pure CO_2. For example, the pressure increased from 1.08 MPa to 5.03 MPa at 303.15 K, whereas the solubility increased only from 0.6331 mol/kg to 7.9775 mol/kg. In addition, the pressure increased from 5.03 MPa to 7.00 MPa, whereas the solubility increased dramatically from 7.9775 mol/kg to 30.7314 mol/kg. This indicated that the CO_2 + n-dodecane system reached the miscible phase with increasing pressure, thereby making the solubility value change significantly with increasing pressure (Lashkarbolooki et al., 2017). In contrast, at lower pressure, the CO_2 solubility in n-dodecane decreased with increasing temperature. The temperature increased from 303.15 to 353.15 K at 5.03 MPa, resulting in a decrease in the solubility of CO_2 in n-dodecane from 7.9775 mol/kg to 1.6270 mol/kg. Studies have shown that increasing temperature can increase the distance between the CO_2 and alkane molecules, reduce their interactions, enhance the Brownian motion of the CO_2 molecules, and allow the CO_2 molecules to escape from the liquid phase, which reduces the CO_2 solubility (Yang et al., 2012).

The CO_2 solubilities in n-dodecane obtained in this study were compared with those reported previously (Fig. 11). Our CO_2 solubility data were basically consistent with the experimental data of Henni et al. (1996) and Brain Bufkin (1986) at pressures below 4.00 MPa. However, at higher pressures, our data show higher CO_2 solubility than those published in the literature, except at 353.15 K. The reasons of lower solubility may be that the system did not reach phase equilibrium while analyzing the results during their experiments. Another reason may be that previous studies need to extract sample fluids, which may disrupt the original equilibrium condition of the system, lead to the escape of CO_2. In addition, the CO_2 solubility becomes more sensitive to the changes of pressure and temperature when the *P-T* conditions are near the critical point of CO_2.

3.4. Solubility prediction model for a CO_2 + n-dodecane system

In CO_2-EOR technology, CO_2 solubility is one of the most important factors required to improve oil recovery. Because of a

lack of experimental data for CO_2 solubility in a wider range of temperatures and pressures, semi-empirical models often have been adopted in previous studies (Tsuji et al., 2004) to predict CO_2 solubility in organic liquids. Jou and Mather (2005) fitted a CO_2 solubility model based on experimental data, as shown in Eq. (3).

$$\ln P = A + B(\ln S) \tag{3}$$

where P is the pressure (MPa); S is the CO_2 solubility (mol/kg); and A and B are functions of the temperature T.

The model is relatively simple and suitable for predicting the solubility of CO_2 in different solvents. Fornari et al. (2009), Paninho et al. (2013), and Howlader et al. (2017) used this model to determine the solubility of CO_2 in organic liquids, such as ethyl lactate and triglycerides. The prediction results were in good agreement with the experimental results. Therefore, this model was also used in this work to predict the solubility of CO_2 in n-dodecane.

In this study, the model developed by Jou and Mather (2005) was improved, as shown in Eq. (4). First, the experimental CO_2 solubilities were fitted with pressure, P, under isothermal conditions. Then, based on the improved model, the relationships among A, B, and T were obtained, as shown in Eqs. (5) and (6). Thus, the CO_2 solubility correlation model obtained by correlating the temperature and pressure was determined to be as following:

$$\ln S = (P - A)/B \tag{4}$$

$$A = -8 \times 10^{-6}T^2 + 0.0354T - 8.1605 \tag{5}$$

$$B = 0.0405T - 10.756 \tag{6}$$

The CO_2 solubility calculated using the prediction model (Fig. 12) were consistent with the experimental data, and the mean average percentage error between the experimental and calculated data was within 4.0%. Therefore, the model can be expanded in future work to predict the CO_2 solubility in a wider range of temperatures and pressures.

4. Conclusions

In this study, to determine the solubility of CO_2 in n-dodecane under near-critical and supercritical conditions ($T = 303.15-353.15$ K, $P \leq 11.00$ MPa), an integrated fused silica capillary and in-situ Raman spectroscopy system was built. The calculated Raman peak intensity ratio was used to qualitatively and quantitatively analyze the CO_2 and its concentrations. The relationship between the known CO_2 molality in the n-dodecane and the Raman intensity ratio, I_{CO_2}/I_{C-H}, was used to establish the correlation equation. Subsequently, the CO_2 solubility of the system was calculated by incorporating the measured I_{CO_2}/I_{C-H} ratio into the correlation equation. The maximum CO_2 solubility (30.7314 mol/kg) was obtained at 303.15 K and 7.00 MPa. Finally, a solubility correlation model ($\ln S = (P - A)/B$) based on the relationship between temperature and pressure was developed. The CO_2 solubility data can be extended using the model equation to provide an empirical correlation and experimental data for the CO_2-EOR technology. This is a promising method for the determination of CO_2 solubility in organic liquids under supercritical conditions of CO_2, provided the occasionally encountered interference of fluorescence on Raman signals can be effectively reduced.

Declaration of competing interest

The authors declare no competing financial interests.

Appendix A. Supplementary data

Supplementary data to this article can be found online at https://doi.org/10.1016/j.petsci.2022.06.014.

References

Awan, A.R., Teigland, R., Kleppe, J., 2008. A survey of North Sea enhanced-oil recovery projects initiated during the years 1975 to 2005. SPE Reservoir Eval. Eng. 11 (3), 497–512. https://doi.org/10.2118/99546-pa.

Bei, K., Wang, J.L., Zhou, S.Y., et al., 2018. Determining the volume expansion of the CO_2 + octane mixture using a fused silica capillary cell with in-situ Raman spectroscopy. J. CO_2 Util. 24, 149–156. https://doi.org/10.1016/j.jcou.2017.12.011.

Belgodere, C., Dubessy, J., Vautrin, D., et al., 2015. Experimental determination of CO_2 diffusion coefficient in aqueous solutions under pressure at room temperature via Raman spectroscopy: impact of salinity (NaCl). J. Raman Spectrosc. 46 (10), 1025–1032. https://doi.org/10.1002/jrs.4742.

Bufkin, B., 1986. High-pressure Solubilities of Carbon Dioxide and Ethane in Selected Paraffinic, Naphthenic and Aromatic Solvents. Oklahoma State University. https://hdl.handle.net/11244/15787.

Caumon, M.C., Dubessy, J., Robert, P., et al., 2017. Microreactors to measure solubilities in the CO_2-H_2O-NaCl system. Energy Proc. 114, 4843–4850. https://doi.org/10.1016/j.egypro.2017.03.1624.

Chung, F.T.H., Jones, R.A., Nguyen, H.T., 1988. Measurements and correlations of the physical properties of CO_2-heavy crude oil mixtures. SPE Reservoir Eng. 3 (3), 822–828. https://doi.org/10.2118/15080-PA.

Cormos, C.C., 2012. Integrated assessment of IGCC power generation technology with carbon capture and storage (CCS). Energy 42 (1), 434–445. https://doi.org/10.1016/j.energy.2012.03.025.

Fornari, T., Hernández, E.J., Reglero, G., 2009. Solubility of supercritical gases in organic liquids. J. Supercrit. Fluids. 51 (2), 115–122. https://doi.org/10.1016/j.supflu.2009.08.015.

Forte, E., Galindo, A., Trusler, J.P.M., 2011. Experimental and molecular modeling study of the three-phase behavior of (n-decane + carbon dioxide + water) at reservoir conditions. J. Phys. Chem. B 115 (49), 14591–14609. https://doi.org/10.1021/jp206806a.

Gui, X., Wang, W., Gao, Q., et al., 2017. Measurement and correlation of high-pressure phase equilibria for CO_2 + alkanes and CO_2 + crude oil systems. J. Chem. Eng. Data 62 (11), 3807–3822. https://doi.org/10.1021/acs.jced.7b00517.

Guo, H.R., Chen, Y., Hu, Q.C., et al., 2014. Quantitative Raman spectroscopic investigation of geo-fluids high-pressure phase equilibria: Part I. Accurate calibration and determination of CO_2 solubility in water from 273.15 to 573.15 K and from 10 to 120 MPa. Fluid Phase Equil. 382, 70–79. https://doi.org/10.1016/j.fluid.2014.08.032.

Han, H.S., Yuan, S.Y., Li, S., et al., 2015. Dissolving capacity and volume expansion of carbon dioxide in chain n-alkanes. Petrol. Explor. Dev. 42 (1), 97–103. https://doi.org/10.1016/S1876-3804(15)60011-8.

Henni, A., Jaffer, S., Mather, A.E., 1996. Solubility of N_2O and CO_2 in n-dodecane. Can. J. Chem. Eng. 74 (4), 554–557. https://doi.org/10.1002/cjce.5450740418.

Hill, B., Hovorka, S., Melzer, S., 2013. Geologic carbon storage through Enhanced oil recovery. Energy Proc. 37, 6808–6830. https://doi.org/10.1016/j.egypro.2013.06.614.

Howlader, M.S., French, W.T., Toghiani, H., et al., 2017. Measurement and correlation of solubility of carbon dioxide in triglycerides. J. Chem. Thermodyn. 104, 252–260. https://doi.org/10.1016/j.jct.2016.09.035.

Jou, F.Y., Mather, A.E., 2005. Solubility of carbon dioxide in an aqueous mixture of methyldiethanolamine and N-methylpyrrolidone at elevated pressures. Fluid Phase Equil. 228–229, 465–469. https://doi.org/10.1016/j.fluid.2004.10.004.

Kavousi, A., Torabi, F., Chan, C.W., et al., 2014. Experimental measurement and parametric study of CO_2 solubility and molecular diffusivity in heavy crude oil systems. Fluid Phase Equil. 371, 57–66. https://doi.org/10.1016/j.fluid.2014.03.007.

Lacy, R., Serralde, C., Climent, M., et al., 2013. Initial assessment of the potential for future CCUS with EOR projects in Mexico using CO_2 captured from fossil fuel industrial plants. Int. J. Greenh. Gas Control 19, 212–219. https://doi.org/10.1016/j.ijggc.2013.07.017.

Lashkarbolooki, M., Eftekhari, M.J., Najimi, S., et al., 2017. Minimum miscibility pressure of CO_2 and crude oil during CO_2 injection in the reservoir. J. Supercrit. Fluids 127, 121–128. https://doi.org/10.1016/j.supflu.2017.04.005.

Lay, E.N., Taghikhani, V., Ghotbi, C., 2006. Measurement and correlation of CO_2 solubility in the systems of CO_2 + Toluene, CO_2 + Benzene, and CO_2 + n-Hexane

at near-critical and supercritical conditions. J. Chem. Eng. Data 51 (6), 2197–2200. https://doi.org/10.1021/je0602972.

Leung, D.Y.C., Caramanna, G., Maroto-Valer, M.M., 2014. An overview of current status of carbon dioxide capture and storage technologies. Renew. Sustain. Energy Rev. 39, 426–443. https://doi.org/10.1016/j.rser.2014.07.093.

Li, S.Y., Li, Z.M., Dong, Q.W., 2016. Diffusion coefficients of supercritical CO_2 in oil-saturated cores under low permeability reservoir conditions. J. CO_2 Util. 14, 47–60. https://doi.org/10.1016/j.jcou.2016.02.002.

Liu, B., Shi, J.Q., Wang, M.H., et al., 2016. Reduction in interfacial tension of water–oil interface by supercritical CO_2 in enhanced oil recovery processes studied with Molecular Dynamics Simulation. J. Supercrit. Fluids 111, 171–178. https://doi.org/10.1016/j.supflu.2015.11.001.

Liu, N., Aymonier, C., Lecoutre, C., et al., 2012. Microfluidic approach for studying CO_2 solubility in water and brine using confocal Raman spectroscopy. Chem. Phys. Lett. 551, 139–143. https://doi.org/10.1016/j.cplett.2012.09.007.

Lv, G.Z., Li, Q., Wang, S.J., et al., 2015. Key techniques of reservoir engineering and injection–production process for CO_2 flooding in China's SINOPEC Shengli Oilfield. J. CO_2 Util. 11, 31–40. https://doi.org/10.1016/j.jcou.2014.12.007.

Michael, K., Golab, A., Shulakova, V., et al., 2010. Geological storage of CO_2 in saline aquifers—a review of the experience from existing storage operations. Int. J. Greenh. Gas Control 4 (4), 659–667. https://doi.org/10.1016/j.ijggc.2009.12.011.

Mosavat, N., Abedini, A., Torabi, F., 2014. Phase behaviour of CO_2–brine and CO_2–oil systems for CO_2 storage and enhanced oil recovery: experimental studies. Energy Proc. 63, 5631–5645. https://doi.org/10.1016/j.egypro.2014.11.596.

Nourozieh, H., Kariznovi, M., Abedi, J., 2013. Measurement and correlation of saturated liquid properties and gas solubility for decane, tetradecane and their binary mixtures saturated with carbon dioxide. Fluid Phase Equil. 337, 246–254. https://doi.org/10.1016/j.fluid.2012.09.037.

Paninho, A.B., Nunes, A.V.M., Paiva, A., et al., 2013. High pressure phase behavior of the binary system (ethyl lactate + carbon dioxide). Fluid Phase Equil. 360, 129–133. https://doi.org/10.1016/j.fluid.2013.09.024.

Pan, Z.Y., Ma, Y.P., Chou, I.M., 2013a. Solubility of 2,4-dichlorotoluene in water determined in fused silica capillary reactor by in situ Raman spectroscopy. AIChE J. 59 (8), 2721–2725. https://doi.org/10.1002/aic.14163.

Pan, Z.Y., Shi, Y.H., Liu, L., et al., 2013b. Depolymerization of poly (butylene terephthalate) in sub- and supercritical ethanol in a fused silica capillary reactor or autoclave reactor. Polym. Degrad. Stabil. 98 (7), 1287–1292. https://doi.org/10.1016/j.polymdegradstab.2013.04.004.

Peng, C., Crawshaw, J.P., Maitland, G.C., et al., 2013. The pH of CO_2-saturated water at temperatures between 308 K and 423 K at pressures up to 15 MPa. J. Supercrit. Fluids 82, 129–137. https://doi.org/10.1016/j.supflu.2013.07.001.

Sun, L.L., Dou, H.G., Li, Z.P., et al., 2017. Assessment of CO_2 storage potential and carbon capture, utilization and storage prospect in China. J. Energy Inst. 91 (6), 970–977. https://doi.org/10.1016/j.joei.2017.08.002.

Tsuji, T., Tanaka, S., Hiaki, T., et al., 2004. Measurements of bubble point pressure for CO_2 + decane and CO_2 + lubricating oil. Fluid Phase Equil. 219 (1), 87–92. https://doi.org/10.1016/j.fluid.2004.01.019.

Wang, J.L., He, B.B., Xie, L.F., et al., 2019. Determination of CO_2 solubility in water and NaCl solutions under geological sequestration conditions using a fused silica capillary cell with in Situ Raman spectroscopy. J. Chem. Eng. Data 64 (6), 2484–2496. https://doi.org/10.1021/acs.jced.9b00013.

Wang, J.L., Zhou, S.Y., Bei, K., et al., 2017a. A new approach for the measurement of the volume expansion of a CO_2 + n-dodecane mixture in a fused silica capillary cell by Raman spectroscopy. Fuel 203, 113–119. https://doi.org/10.1016/j.fuel.2017.04.094.

Wang, J.L., Zhou, S.Y., Bei, K., et al., 2017b. Using a fused silica capillary cell and in situ Raman spectroscopy to develop a setup for measurement of the volume expansion of carbon dioxide + n-hexane. Energy Fuel. 31 (6), 6314–6319. https://doi.org/10.1021/acs.energyfuels.7b00549.

Wang, Z., Zhou, Q., Guo, H.R., et al., 2018. Determination of water solubility in supercritical CO_2 from 313.15 to 473.15 K and from 10 to 50 MPa by in-situ quantitative Raman spectroscopy. Fluid Phase Equil. 476 (Part B), 170–178. https://doi.org/10.1016/j.fluid.2018.08.006.

Yang, Z.H., Li, M.Y., Peng, B., et al., 2012. Dispersion property of CO_2 in oil. 1. Volume expansion of CO_2 + alkane at near critical and supercritical condition of CO_2. J. Chem. Eng. Data 57 (3), 882–889. https://doi.org/10.1021/je201114g.

Yang, Z.H., Li, M.Y., Peng, B., et al., 2013. Volume expansion of CO_2 + oil at near critical and supercritical conditions of CO_2. Fuel 112, 283–288. https://doi.org/10.1016/j.fuel.2013.04.037.

You, H., Seo, Y., Huh, C., et al., 2014. Performance analysis of cold energy recovery from CO_2 injection in ship-based carbon capture and storage (CCS). Energies 7 (11), 7266–7281. https://doi.org/10.3390/en7117266.